Analyst

Comparison of the Different Responses of Quartz Crystal Microbalance and Surface Plasmon Resonance under Various Experimental Scenarios at Solid-Liquid Interfaces

Journal:	*Analyst*
Manuscript ID:	AN-ART-09-2014-001756.R1
Article Type:	Paper
Date Submitted by the Author:	02-Dec-2014
Complete List of Authors:	Fang, Jiajie; Nanjing University, Departmen of Physics Jiang, Zhongying; Nanjing University, Department of Physics Zhu, Tao; Nanjing University, Department of Physics Ren, Chunlai; Nanjing University, Physics Ma, Yu-qiang; Nanjing University, Department of Physics Wang, Kaiyu; Nanjing University, Department of Physics

Table of Content Entry

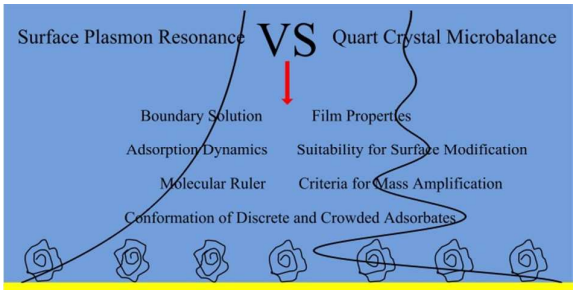

The different characters of surface plasmon resonance and quartz crystal microbalance techniques under different experimental scenarios were discussed.

Comparison of the Different Responses of Surface Plasmon Resonance and Quartz Crystal Microbalance under Various Experimental Scenarios at Solid-Liquid Interfaces

Jiajie Fang,[†] *Chunlai Ren,*[†] *Tao Zhu,*[†] *Kaiyu Wang,*[†] *Zhongying Jiang,*[‡†*] *Yuqiang Ma*[†§*]

[†]National Laboratory of Solid State Microstructures and Department of Physics, Nanjing University, Nanjing 210093, China

[‡]School of Electronics and Information and College of Chemistry and Biological Science, Yi Li Normal University, Yining 83500, China

[§]Laboratory of Soft Condensed Matter Physics and Interdisciplinary Research, Soochow University, Suzhou 215006, China

[*]Authors to whom correspondence should be addressed. Tel and e-mail: (086)13813955964; jiangzhying@163.com(Z. Y. Jiang) and (086)02583592900, myqiang@nju.edu.cn(Y. Q. Ma).

ABSTRACT: The ability to obtain a molecular-level understanding of phenomena at solid-liquid interfaces, ranging from mass to conformation change, is the key to developing and improving many chemical and biological systems, as well as scientific and medical applications. Surface plasmon resonance (SPR) and quartz crystal microbalance (QCM) techniques are frequently coupled to achieve this ability. In this work, we divided the various experimentally relevant scenarios into the following six categories: boundary solution, surface modification, conformation, viscoelastic properties, molecular ruler, and mass sensitivity. For each case, based upon theoretical analysis, we discuss the following four points: (1) the different types of information that can be obtained, why it can be obtained, and how to obtain it, (2) the origins of many current approaches and why they are imperfect, (3) the guidelines for experimental design, and (4) the possible studies, such as the effect of dimensional confinement and adsorption force on the ability of conformational change to occur upon receiving external stimuli and the hysteresis in this change, of discrete adsorbates at solid-liquid interfaces.

I INTRODUCTION

Phenomena such as the adsorption of polymers and biomolecules onto solid-liquid interfaces, and the conformational change of adsorbates upon receiving external stimuli, are prevalent in nature and central to many chemical and biological processes, as well as scientific and medical applications. The adsorption (deposition, adhesion) of biomolecules onto blood vessel, oral tissues, and cells, etc., may result in many diseases (infectious diseases, idiopathic dilated cardiomyopathy, stroke, etc.).[1] However, the adsorption of polyelectrolyte

onto these systems has a variety of biomedical applications,[2] such as in vivo repair of damaged blood vessels.[3] The biocompatibility of implants and in vivo sensors is dominated by the conformation of adsorbed proteins on their surfaces.[4] The conformational change of polymers at solid-liquid interfaces, in accordance with external stimuli, offers exciting possibilities for the fabrication of adaptive, responsive, and smart interfaces.[5] This capability is relevant to many biotechnological and biomedical applications, and has attracted considerable interest for developing a range of sensors, including chemical gratings, microgravimetric, micromechanical, and optical transduction of chemical signals.[5]

The ability to obtain a molecular-level understanding of such phenomena is the key to developing and improving these chemical and biological systems, as well as scientific and industrial applications. However, this remains a formidable challenge. The information of polymers and biomolecules at solid-liquid interfaces is much richer than that at solid-vapor interfaces or in bulk solution. For instance, they have a variety of conformations and orientations,[6] which rely heavily on the surface coverage, solvent quality, strength of molecule-substrate interaction, molecular weight, etc.

One possible method to obtain such ability is to combine different techniques. Amongst all of the combinations of related techniques, the alliance of quartz crystal microbalance (QCM) and one mass sensor, mostly surface plasmon resonance (SPR) [7,8,10-14] and sometimes ellipsometry,[9,15-18] is very attractive. This combination can provide a wealth of information on adsorbates, including the areal mass, film thickness, hydrodynamic effects, viscosity and shear modulus, conformation (rupture of adsorbed intact vesicles and formation of bilayer, etc.), local mechanical properties, size, height-to-width ratio, lateral distribution, and intrinsic

viscosity.[7-19] SPR and QCM techniques can share the same sensor surface, and have the significant flexibility for designing thin film platforms. They are relatively easy to use. They work in the liquid phase, and can monitor the changes in situ with a reasonable time resolution and high sensitivity, without requiring labels, etc.

The combination of different techniques to obtain as much information as possible requires an in-depth understanding of the response mechanisms and data analysis under different conditions. The data analysis of SPR is relatively simple. A detailed description of this sensor can be found in SI 1. It consists of a transparent optical substrate coated with a thin (~ 50 nm) metallic (Au, or Silver, etc.) film. When light propagates from the substrate to the film, total reflection occurs if the incident angel is larger than the critical angle, and an evanescent field is generated in the film.[20-22] When this wave couples with the electron (surface plamson) in the film surface to drive them to resonant, the intensity of the reflected light is significantly reduced.[20-22] This critical incident angle θ is the SPR signal. Although θ has been reported to measure the conformational change of adsorbed layer,[23] in general $\Delta\theta$ is proportional to the mass change on top of metallic film **(**eq S3**)**, Δm.[7,8,10-14] From the mass estimation, other information like the structural properties of adsorbed layers (thickness, surface concentration, fractional coverage, etc.) can be obtained.[22] However, it is not very clear for determining certain characteristics under specific conditions, such as the criteria for mass amplification and sensitivity improvement.

The data analysis of the QCM is extremely complex. The technique comprises a thin quartz crystal sandwiched between two metal electrodes that establish an alternating electric field across the crystal, causing vibrational motion of the crystal at its resonant frequency (SI

1). This frequency is the QCM signal. In gas phase, the Sauerbrey equation is valid, $\Delta f/\Delta m = -f/m_q$, where m_q is the areal mass of quartz crystal.[24] In liquid phase, however, with increasing Δm, $\Delta f/\Delta m$ may remain constant, with large fluctuations depending on the species,[25] or decreases monotonically, with varying functions to maintain the ratio.[12,15,16,18] Although many models have been developed for modeling QCM signal,[26-29] a simple and direct relation between Δf and Δm has not been realized until one of soon to be published studies.[19] Furthermore, these models are difficult to use because of their complex form, questionable preconditions, etc. The simple approximations and empirical models,[8,12,15,16,18,30-32] such as the finite element method simulation[16] and trapped liquid coat model,[15,18] are phenomenological and valid only in some specific cases. Therefore, an in-depth illustration of the physics of QCM technique in different scenarios has not been published.

In the past several years, using QCM technique we measured adsorption of polymer[33] and nanoparticles,[34] and desorption of lysozyme,[35] revealed the effect of calcium cation on lipid vesicle deposition and osmotic stress on membrane fusion,[36] investigated the lipid exchange between membranes,[37] probed the viscosity of boundary polymer solution of tens of nanometers size.[38] We also numerically calculated the responses of SPR and QCM techniques to the properties of adsorbed layer,[39] and exploited the origins of the different responses.[40] The comprehensive understanding of SPR and QCM techniques coming from these studies enables us to formulate guidelines for approaching SPR and QCM data interpretations for various experimentally related conditions. The scenarios are divided into six following cases: boundary solution, surface modification, conformational characterization, viscoelastic properties, molecular ruler (contacting surfaces), and mass sensitivity. In every case, based

upon the theoretical analysis, we show: (1) what types of information can be obtained, and how to obtain it, (2) the limitation of many current interpretations, and our new understanding, (3) the guidelines for proper experimental design, and (4) the potential interesting studies, as well as the significance of these studies.

II BOUNDARY SOLUTION

The simplest application of SPR and QCM is to measure the refractive index and viscosity of a Newtonian fluid,[22,40] respectively. In this case, the shear acoustic and evanescent waves dissipate their energies in a homogeneous medium. The measured thickness is represented by the characteristic decay length, l_d,[21,22] and the penetration depth, δ (the distance into the liquid where the wave amplitude has fallen by a factor of e), respectively[26,27]

$$l_d = \frac{\lambda}{2\pi}\sqrt{-\frac{\varepsilon_b + \varepsilon_m}{\varepsilon_b^2}} \quad (1)$$

$$\delta = \sqrt{\frac{2\eta_b}{\rho_b \omega}} \quad (2)$$

where λ, ε, η, and ρ are the incident light wavelength, dielectric constant, viscosity and density, respectively, $\omega = 2\pi f$ is the angular frequency, subscript b and m indicate the bulk solution and metallic film, respectively.

Using Fresnel equation and Voight model (equations S1 and S6), we calculated the SPR and QCM responses versus a solution's refractive index and viscosity, respectively (Figure 1). For SPR, $\Delta\theta$ increases proportionally with increasing n (Figure 1A). This agrees with the following equation, which was simplified with Fresnel equation

$$\Delta\theta \approx \frac{4\pi}{\lambda n_b^2 \cos\theta}\left(\frac{\varepsilon_m \varepsilon_b}{\varepsilon_m + \varepsilon_b}\right)^2 \frac{1}{\sqrt{-\varepsilon_b \varepsilon_m}} \frac{l_d}{2} \Delta n \quad (3)$$

From equations S3 and 3 above, for a semi-infinite solution, SPR technique measures the refractive index in the regime $l_d/2$, using the same equation for a thin adsorbed layer.

Δf increases linearly with viscosity in a double logarithmic scale (Figure 1B). This is consistent with the Kanazawa-Gorden equation[42]

$$\Delta f = -\frac{1}{2\pi m_q}\sqrt{\frac{\rho \eta}{2}} \quad (4)$$

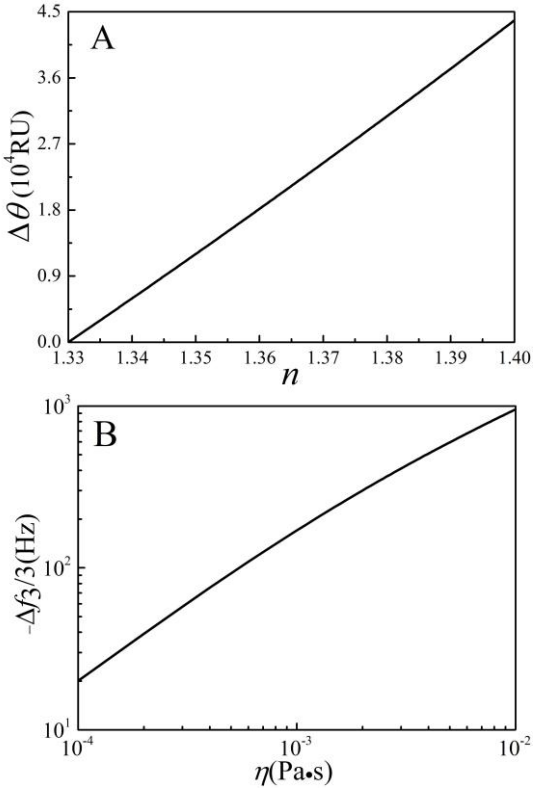

Fig. 1 SPR (A) and QCM (B) responses versus the refractive index and viscosity of a semi-infinite solution. λ = 632.8 nm, ε_p = 3.24, h_m = 50 nm, ε_m = -18.04, f = 15 MHz. The solution of n = 1.33 and η = 0.001 Pa·s is used as the reference. The overtone of resonant frequency is 3.

Equation 4 is a simple method to estimate the validity of QCM data. It implies that for such

a solution, the Sauerbrey equation (equation S5) remains valid, with a new definition of the mass

$$\Delta m = \frac{\rho}{2}\sqrt{\frac{2\eta}{\rho\omega}} = \frac{\rho}{2}\delta \tag{5}$$

This is the same as SPR technique under the same condition.

From the results in Figure 1, for a dilute aqueous solution at 20 °C ($\rho \approx 1.0$ g/cm^3, $\eta \approx 1.0$ mPa·s, n = 1.33) and f = 5 MHz, a 0.1 RU and 0.1 Hz shift (the maximum resolution of current commercial equipment) in θ and f indicate a 1.6×10^{-7} and 1.6×10^{-4} mPa·s change in refractive index and viscosity, respectively. These correspond to the detection limit of 0.8 and 5.33 μg/mL in the case of a refractive index increment of 0.2 mL/g and an intrinsic viscosity of 30 mL/mg, respectively.

For a viscoelastic fluid, both viscosity and shear modulus affect the propagation of shear acoustic wave, and so the energy dissipation will be complex. The Voight model shows that:

$$\Delta f = -\frac{1}{2\pi m_q}\sqrt{\frac{\rho}{2}}\left\{\eta\omega\sqrt{\frac{\sqrt{\mu^2+\eta^2\omega^2}+\mu}{\mu^2+\eta^2\omega^2}} - \mu\sqrt{\frac{\sqrt{\mu^2+\eta^2\omega^2}-\mu}{\mu^2+\eta^2\omega^2}}\right\} \tag{6}$$

$$\Delta D = \frac{1}{\pi f m_q}\sqrt{\frac{\rho}{2}}\left\{\eta\omega\sqrt{\frac{\sqrt{\mu^2+\eta^2\omega^2}-\mu}{\mu^2+\eta^2\omega^2}} + \mu\sqrt{\frac{\sqrt{\mu^2+\eta^2\omega^2}+\mu}{\mu^2+\eta^2\omega^2}}\right\} \tag{7}$$

If ρ is known beforehand, then it is very easy to calculate the solution's viscosity and shear modulus.[38]

A solution measured by SPR and QCM under these conditions can be defined as a boundary solution, as the effective thickness is on the scale of $l_d/2$ and $\delta/2$, respectively. In the past, this type of solution was generally regarded as the bulk. This may come from that in most cases the semi-infinite solution is extra-diluted, of which the viscosity, density and

refractive index approach the solvent. If the solution is semi-dilute, this consideration may be not valid.

The refractive index is a result of the local polarizability of the atoms and chemical groups, which is due to the deformation of the electron configuration about the nuclei, and therefore, it is insensitive to the long-range structure of polymers. The refractive index of a boundary solution is the same as that of bulk solution.

The motion of a polymer relies heavily on its long-range structure, and can be significantly altered by the size of the environment. For polymer films on solid-vapor or liquid-vapor interfaces, the film viscosity depends strongly on the thickness smaller than about 100 nm.[38(c)] This critical value is on the scale of δ in a viscous solution, as shown in Table 1. Similarly, the viscoelastic properties of a boundary polymer solution may differ from the bulk solution. By varying the value of δ, which can be realized by changing *f*, the viscosity profile of a longitudinal concentration homogeneous polymer solution can be obtained. Our recent results showed that for a dilute boundary solution of PEG (molecular weight of 20 k), the viscosity decreases with increasing solution thickness, suggesting that the boundary solution closer to the solid substrate has a larger viscosity.[38(c)]

Furthermore, by probing the dependence of a in the formula $[\eta] = KM^a$ on boundary solution thickness, an understanding of the effect of nanometer size scale of the environment on the conformation of discrete polymers or biomolecules can be developed. Here $[\eta]$ is the linear coefficient in the relation between viscosity and concentration. Such linear relation for boundary polymer solution has already been proved.[38(c)]

In summary, for a boundary solution, SPR is a refractive index and concentration sensor,

while QCM can be used to obtain information relating to the viscoelastic properties of polymer solutions, and reveal the effect of size and confinement at the nanometer size scale on the conformation of discrete polymers and biomolecules near a solid-liquid interface.

Table 1 The characteristic decay length of evanescent electromagnetic field, and the penetration depth of shear acoustic wave in different mediums (f = 5 MHz, ε_m = -18.04).

	Parameters (ρ: g/cm^3, η: mPa·s)	l_d/λ	δ(nm)
Gas	$\rho \sim 10^{-3}$, $\eta \sim 10^{-3}$, $\varepsilon \sim 1$	~ 0.657	~ 252
Viscous solution	$\rho \sim 1$, $\eta \sim 1$, $\varepsilon \sim 1.82$	~ 0.475	~ 252
Viscoelastic medium	$\rho \sim 1$, $\eta \sim 10$, $\varepsilon \sim 2.25$	~ 0.422	~ 800
Solid film	$\rho \sim 1$, $\eta \to \infty$, $\varepsilon \sim 3.24$	~ 0.312	$\to \infty$

III SURFACE MODIFICATION

One of the greatest advantages of SPR and QCM is their significant flexibility for designing various film platforms. Before testing the efficiency of one platform, its influence on SPR and QCM signals should be accurately evaluated. The dependences of SPR and QCM signals on properties (thickness, refractive index, viscosity, and their profiles) of the modified layer are shown in Figures S2, S3 and S4. The similar behaviors can also be found elsewhere.[22,27,39] In brief, in thin film limit, SPR signal is proportional to the refractive index shift ($\int(n_f(z) - n_b)dz$) of the film. On the contrary, QCM signal depends strongly on the specific value of surface layer viscosity and its profile. These consist with the experimental results.[7,8,12] SI 2 discusses the origins of these different responses.

Therefore, SPR signal is unaffected by the rigidity of the layer. It only requires a thin layer, generally less than tens of nanometers, to avoid the significant energy loss of evanescent wave. The QCM technique prefers a solid layer, since the viscosity profile of a modified layer is expected to be constant. The thickness is infinite in principle, and can be as high as tens of micrometers in practice.

The discussions above are based on the ideal situation, a laterally homogeneous film, for simplified data analysis. However, the layer is often laterally heterogeneous. In this situation, we need to pay attention to whether the desired information can be exploited qualitatively or is unavailable.

For example, it has been widely reported that modifying the surface with nanowires and nanoholes, which are tens to hundreds of nanometers thick, to improve the detection limit.[43] The capture enhancement was monitored by optical microscopy, etc.[43] The downsides of these methods include ex situ measurement, complex experimental operation, etc.

In this situation, evanescent wave dissipates in part or completely in the nanowires and the fluid between them (Figure 2A). The SPR detector measures the change in the fluid's refractive index.

The well between different nanowires or nanoholes can be sealed by the lipid bilayer.[44] SPR technique provides an excellent tool to observe the translocation mechanism of nanoparticles of different shapes, and other functional molecules, across this bilayer. The sensitivity of such technique increases with decreasing nanowires thickness.

These modified surfaces have also been measured by QCM technique.[45] The fluid between the nanowires behaviors as rigid during high shear oscillation, and therefore, the energy loss

of shear acoustic wave in such liquid is negligible (Figure 2B). QCM measures the mass between nanowires, as well as the viscoelastic properties of the layer above the nanowires. The relationship between the properties of the layer above the nanowires and Δf is complex, making such measurement qualitative.

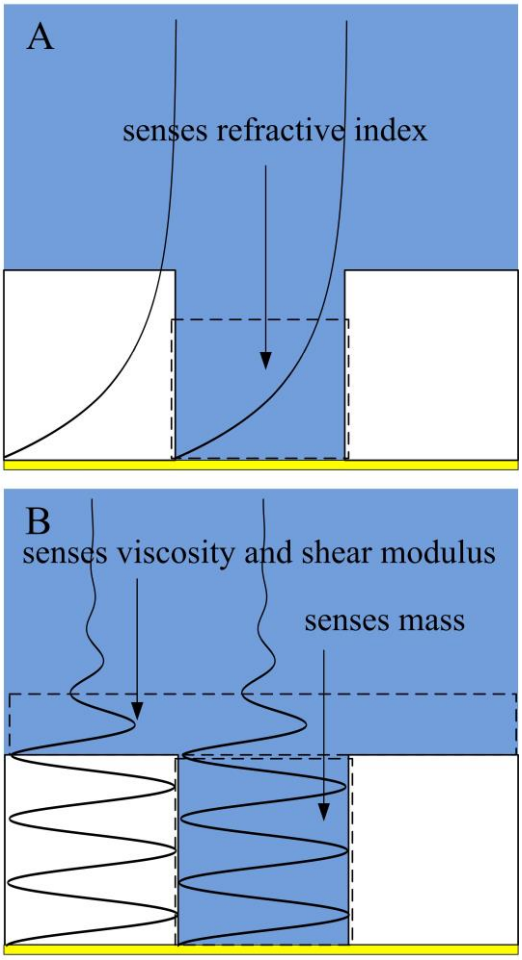

Fig. 2 Different sensitive regimes of SPR (A) and QCM (B) techniques on nanowire modified surfaces.

IV CONFORMATION CHARACTERIZATION

IV.1 SPR: Qualitative Conformation Characterization of Thick Layers

SPR technique has been used to monitor the conformational change of layers at solid-liquid

interfaces.[23] This conflicts with theoretical calculations (Figure S4A, and ref 39(c)) and most experimental results,[7,8,10-14] showing that $\Delta\theta$ is independent of the conformation of adsorbates. The origin of such a difference is that SPR technique is sensitive and inert to the conformational change of thick and thin layers, respectively, as shown in Figure S4.

To establish a relationship between the refractive index of a thick layer and the resulting $\Delta\theta$, similar to equation S3 for the thin layer, a properly weighted factor is required. According to Jung et al.,[21] since light is used to probe the refractive index, it is natural to assume that the proper weighting factor at each point in the layer should be proportional to the intensity of light at that point. The evanescent electromagnetic field decays exponentially into the film, $E(z) = E_0\exp(-z/l_d)$.[21] The intensity of light is the field strength squared, so it decays with distance z into the metal surface as $\exp(-2z/l_d)$. The $\Delta\theta$ of a homogeneous film is thus

$$\Delta\theta \approx \frac{4\pi}{\lambda\cos\theta}\left(\frac{\varepsilon_m}{\varepsilon_m+\varepsilon_b}\right)^2\sqrt{-\frac{\varepsilon_b}{\varepsilon_m}}\frac{dn}{dc}c_f\frac{l_d}{2}\left[1-\exp\left(-\frac{2h_f}{l_d}\right)\right] \quad (8)$$

The validity of this factor has been examined before,[21] and can also be proven here. From Figures S2A and S3A, for a homogeneous bulk solution and a thin film, it has $\Delta\theta = 62.57\ \Delta n$ and $\Delta\theta = 0.474\ \Delta n \times h$ (the unit of h is nm), respectively. Expanding $\Delta\theta = 0.474\Delta n \times h$ to a semi-infinite layer, we have

$$\Delta\theta = 0.474\Delta n\int\exp(-2z/l_d)dz = 0.474 l_d\Delta n/2 \quad (9)$$

where

$$l_d = \frac{\lambda}{2\pi}\sqrt{-\frac{\varepsilon_m+\varepsilon_b}{\varepsilon_b^2}} = 261.52\text{nm} \quad (10)$$

$$\Delta\theta = 61.98\Delta n \quad (11)$$

Therefore, the collapse of adsorbates leads to the increase of the term $c_f[1 - \exp(-2h_f/l_d)]$,

and as a result, the increase of $\Delta\theta$. Swelling is the inverse process of collapse and results in a decrease of $\Delta\theta$.

Since l_d and the size of most polymers (biomolecules) are approximately two hundred and several to tens of nanometers, respectively, the conformational change of adsorbates generally does not affect $\Delta\theta$. This is why SPR signal is usually insensitive to the conformation of adsorbed molecules. However, for the case of polymer brushes, where the polymers are extensively stretched, $\Delta\theta$ depends on the conformation.[23]

Please note that the external stimuli used to produce the conformational change of the adsorbates may also lead to the change of the value of $[\varepsilon_m/(\varepsilon_m + \varepsilon_b)]^2(-\varepsilon_b/\varepsilon_m)^{1/2}dn/dc$. To quantify the conformation information, a new parameter, X, is recommended where:

$$X = \int_0^{h_f} c(z)\exp(-\frac{2z}{l_d})dz = \frac{\Delta\theta}{\frac{4\pi}{\lambda\cos\theta}(\frac{\varepsilon_m}{\varepsilon_m+\varepsilon_b})^2\sqrt{-\frac{\varepsilon_b}{\varepsilon_m}}\frac{dn}{dc}} \quad (12)$$

This new parameter depends only on the conformation (surface concentration profile), since the effects of the external environment are eliminated.

Finally, it should be noted out that this monitoring is qualitative, as it is impossible to establish the relation between $\Delta\theta$ and the properties (concentration and thickness, or concentration profile) of adsorbed layer at solid-liquid interfaces. In case of a homogeneous layer with known total mass, the film thickness can be obtained from equation 8.

IV.2 QCM: Qualitative Conformation Characterization by the Variation of Δf with Fixed Surface Mass.

QCM technique has become popular for studying the conformation of chains at solid-liquid interfaces.[7-18,46-48] The ability to take in situ conformation measurement is one of the greatest

advantages of QCM technique. Unlike evanescent wave, the energy loss of shear acoustic wave in a thick layer is neglected, as the thick layer generally has a rigid inner-layer. The sensitivity of QCM technique to the conformation of molecules at solid-liquid interfaces cannot be attributed to the decreasing sensitivity of shear acoustic wave with increasing distance to the sensor surface. This is proven with the results shown in Figure S4. The same form of conformational change results in the same variation of Δf, regardless of layer thickness.

Furthermore, QCM technique offers Δf and ΔD (SI 1).[26,27] The change of Δf, the relationships between ΔD ($\Delta D/(-\Delta f)$) and Δf, and between Δf and Δm, can all be used to probe the conformation of chains at solid-liquid interfaces. However, a clear, definitive explanation remains a formidable challenge, because of the rambling experimental results.

Concerning the change of Δf, the most widely accepted explanation is that QCM technique measures the wet mass

$$\Delta f = -\frac{f}{m_{\mathrm{q}}}\Delta m_{\mathrm{wet}} \tag{13}$$

where

$$\Delta m_{\mathrm{wet}} = \Delta m_{\mathrm{ads}} + \Delta m_{\mathrm{solvent}} \tag{14}$$

During conformation changes, the amount of solvent interacting strongly with the chains also varies.

In this section, we offer another interpretation based on the Voight model and the relationship between surface viscosity and concentration. The distance to the sensor surface and the thickness of sub-layer 1 is h and Δh ($\Delta h << h << \delta$), respectively. Sub-layer 2 is above sub-layer 1, and is the same thickness. Their properties are proposed to be the same, c_{f1}

= c_{f2}, $\eta_{f1} = \eta_{f2}$, $\rho_{f1} = \rho_{f2}$. For simplicity, the shear modulus is omitted. Their QCM responses are[27]

$$\Delta f_1 = \Delta f_2 = -\frac{\rho_f \Delta h}{m_q}[1-\frac{\eta_b}{\eta_{f1}}]f \quad (15)$$

For a chain in sub-layer 2 entering sub-layer 1, then

$$\Delta f_1^{'} = -\frac{\rho_f \Delta h}{m_q}[1-\frac{\eta_b^{'}}{\eta_{f1}^{'}}]f \quad (16)$$

The changing trend relies on the specific values of η_b/η_{f1} and $\eta_b^{'}/\eta_{f1}^{'}$. According to the value of η_b/η_{f1}, two cases are plausible.

Case 1:

$$\eta_{f1} \geq 2\eta_b \quad (17)$$

and therefore

$$\Delta f_1^{'} > -\frac{\rho_f \Delta h}{m_q} f \geq 2\Delta f_1 \quad (18)$$

This means that the collapse of a chain in the semi-dilute or concentrated regime results in a decreases of Δf.

Case 2:

$$\eta_b < \eta_{f1} < 2\eta_b \quad (19)$$

meaning that the layer is dilute. In this case, the relationship between η and c can be written as

$$\eta = (1+\eta_{red}c)\eta_b \quad (20)$$

where η_{red} is the reduced viscosity. We define a new viscosity, $\eta_0^{''} = [1+\eta_{red}^{''}2c_{f1}]\eta_b^{'}$, which means

$$1-\frac{\eta_{\mathrm{b}}^{'}}{\eta_{0}^{''}}=2(1-\frac{\eta_{\mathrm{b}}}{\eta_{1}}) \tag{21}$$

and therefore

$$\eta_{\mathrm{red}}^{''}=\frac{\eta_{\mathrm{red}1}}{1-\eta_{\mathrm{red}1}c_{\mathrm{f}1}} \tag{22}$$

The changing trend of Δf during the conformational change of discrete adsorbates depends on the specific values of $\eta_{\mathrm{red}1}^{'}$ and $\eta_{\mathrm{red}1}/(1-\eta_{\mathrm{red}1}c_1)$. The quantitative determination of η_{red} for chains at solid-liquid interfaces is hard, but it may have the same conformation dependence as the chain in a bulk solution.

In a dilute polyelectrolyte solution at fixed concentration, with decreasing chain size, which can be realized by increasing salt concentration, η_{red} decreases, too.[49] In a dilute neutral polymer solution, η_{red} reduces to intrinsic viscosity, $[\eta]$, which is independent of concentration and generally regarded as the ratio of the volume occupied by a single molecule to the molecular weight. At the same time, as stated in one of our recent papers, the value of η_{red} for discrete chains at solid-liquid interfaces is dominated by the overall size of a single chain, not the concentration of the sub-layer.[19] As a result, the collapse of chains would result in the decrease of η_{red} and Δf.

Therefore, we provide an alternate model of how QCM could measure the conformational change of chains at solid-liquid interfaces. In this view, the collapse of the adsorbed layer decreases the QCM signal.

The actual situation is more complex, but the conclusion remains. The existence of shear modulus leads to a greater acoustic contrast between the layer and background ($\mu_{\mathrm{f}}^2+\eta_{\mathrm{f}}^2\omega^2>\eta_{\mathrm{f}}^2\omega^2$), and makes case 1 the dominant situation.

In addition, if the surface coverage is small, Δf from adsorbed chains would also be small. It is very difficult to eliminate the signal attenuation by the background. Therefore, the surface coverage in this situation is in general very high, further indicating that case 1 is the most likely situation.

IV.4 QCM: Conformation of Discrete Chains from the Relationship between Δf and Δm.

As stated in the introduction, in liquid phase, the relationship between Δf and Δm is very complex. When Δf is proportional to Δm, the coefficient depends on the species.[25] Two effects are deemed to be responsible for such dependence. One is the bounded water effect.[25(b)] The other is the friction effect.[25(c)] When values of apparent added mass ($\Delta m_{QCM}/\Delta m$ - 1) were plotted against values relating to the friction (antimobility), such as values of the molecular weight divided by the sedimentation coefficient, the inverse of the diffusion coefficient, and the volume divided by the surface area, there were good linear correlations. On the basis of an energy-transfer model, the apparent added mass in the aqueous solution was explained by the frictional effect at the interface between adsorbates and the aqueous solution.

The disproportionate relationship between Δf and Δm has attracted a greater interest as more information can be extracted.

During the vesicle to supported phospholipid bilayer formation process and streptavidin binding on top of a biotin-modified lipid bilayer, Δf decreases with increasing Δm.[12] Reimhult et al. attributed this decrease to the temporal variation in the coupled water mass per adsorbed biomolecules mass. This mass is defined as

$$\varphi = \frac{m_{\text{Voight}}}{\Delta m} - 1 \tag{23}$$

where m_{Voight} is the mass calculated from Voight model.

During the adsorption process, the surface coverage is usually low. In this case the film is composed of discrete nanosized objected. Johannsmann et al. concluded that the QCM response in such films is governed by hydrodynamic effects and the motion of surface-adsorbed particles.[15,16,32] They have shown that these effects and motion can be modeled empirically[15] and understood fundamentally.[16, 32] From finite element method (FEM) simulation, the stress distribution around the surface-bound particles was calculated and used to derive the frequency and dissipation change.[18,32] With molecular geometry and mechanical parameters as a starting point, the coverage-dependence decrease in sensitivity of QCM in laterally heterogeneous films can be reproduced without the need for fitting parameters.[32]

To interpret the coverage dependent QCM response during the adsorption of Lyophilized streptavidin, lyophilized avidin, cowpea mosaic virus, avidin, AnxX5, AnxA5 mut, etc., Bingen et al. developed a trapped liquid coat model.[15,18] Phenomenological, the hydrodynamically trapped liquid can be rationalized as a coat that surrounds each adsorbed molecule. The fractional trapped liquid is defined as

$$H = 1 - \frac{\Delta m}{\Delta m_{\mathrm{QCM}}} \tag{24}$$

This model relies on an independent measurement of Δm. The fractional trapped liquid H vs Δm, is then fitted. The magnitude of the fractional trapped liquid and the rate of the decrease with increasing coverage are sensitive to the conformation of particle and internal liquid content. If particle weight and lateral distribution are known, the fit yields particle size and height-to-width ratio. If the particle size and orientation on the surface are known, the fit provides information about the lateral distribution of particles. With increasing coverage, these coats increasingly overlap, leading to a decrease in the fractional trapped liquid, and so

does the QCM response.[18]

Common to all these approaches, except friction effect, is that the mass measured by QCM technique includes the trapped liquid. The extent of this trapping is governed by the adsorbate's surface coverage, size, shape, orientation, molecular weight, etc. It also relies on the interactions between the adsorbate and solvent, and substrate.

This hydrodynamic effect concept comes from the hydrodynamic interactions in polymer physics.[6] In dilute bulk solution, these interactions are strong between the monomers and the solvent within the pervaded volume of the chain. When the polymer moves, it effectively drags the solvent within its pervaded volume with it.[6]

This hydrodynamic effect on the QCM signal is useful for qualitative interpretations of why the value of $-\Delta f/\Delta m$ is larger than that in the Sauerbrey equation, and why this value is sensitive to the species of object investigated. However, initially there is no obvious demarcation separating trapped solvent from free solvent. On the other hand, the hydrodynamic effect in dilute solutions can be probed by techniques such as dynamic light scattering,[6] which quantitatively measures the amount of trapped solvent. In addition, these approaches cannot show us the physics of the dependence and independence of $-\Delta f/\Delta m$ on Δm. While the solvated size would decrease with increasing grafting density when the adsorbed chains begin to overlap, it should be fixed once the average distance is much larger than the size itself (i.e., the surface coverage is very low).

We recently found that if the adsorbed film satisfies four preconditions, $\rho_f \approx \rho_b$, $\mu_f << \eta_f\omega$, $\eta_f = (1 + [\eta]c_f)\eta_b$ and $[\eta]c_f << 1$, then[19]

$$\frac{\Delta f}{f} = -\rho_b[\eta]\frac{\Delta m}{m_q} \quad (25)$$

Three of these preconditions, $\rho_f \approx \rho_b$, $\mu_f << \eta_f\omega$ and $[\eta]c_f << 1$ are valid as long as the surface coverage is low, which is the same as the case discussed above. Although equation 25 cannot provide the physics of the specific relationship between φ and Δm, and between H and Δm, it shows that the disproportionate response between Δf and Δm is attributed to the nonlinear relation between surface viscosity and concentration.

Another form of equation 25 is $[\eta] = -(m_q/f\rho_b)\Delta f/\Delta m$, where $m_q/f\rho_b$ can be determined beforehand. Then, from measured $-\Delta f/\Delta m$ and a calibration curve (specifically, multiply by $m_q/f\rho_b$), it is very convenient to obtain the intrinsic viscosity of discrete adsorbates at solid-liquid interfaces, as shown in Figure 3.

The great success of viscosity measurement describing the conformation of discrete polymers and biomolecules in bulk solution[50] has naturally led to using this method to probe the conformation of isolated molecules at solid-liquid interfaces. This idea had not been realized until the formulation of equation 25. From this equation, theories and models to analyze the physical meaning of intrinsic viscosity can be introduced to exploit the information hidden behind the flexible value of $\Delta f/\Delta m$, which contains the special character of the conformation of molecules at solid-liquid interfaces.

In bulk solution, the relationship between the value of a calculated from the formula $[\eta] = KM^a$, and the conformation of a single molecule, has been well-established.[50] For end-grafted molecules, $[\eta]$ estimated by equation 25 is determined by the conformation of the whole molecule, using $[\eta] = KM^a$, too. For weakly physisorbed molecules, $[\eta] = KM^a$ and $[\eta] = KM^0$ are suggested for M smaller (end-grafted on the solid substrate) and larger than that of

an adsorption blob, respectively. A detailed description of the conformation analysis from the value of $\Delta f/\Delta m$ in this case can be found elsewhere.[19]

For a viscous solution (Newtonian liquid), $\Delta f/f = -\Delta m/m_q$, and $\rho[\eta] = 1$ since $\Delta m = \rho\delta/2$. The rough relationship between the conformation (the size of whole chain for end-grafted and adsorption blob for physisorbed) of adsorbate and the value of $-\Delta f/\Delta m$ is shown in Figure 3.

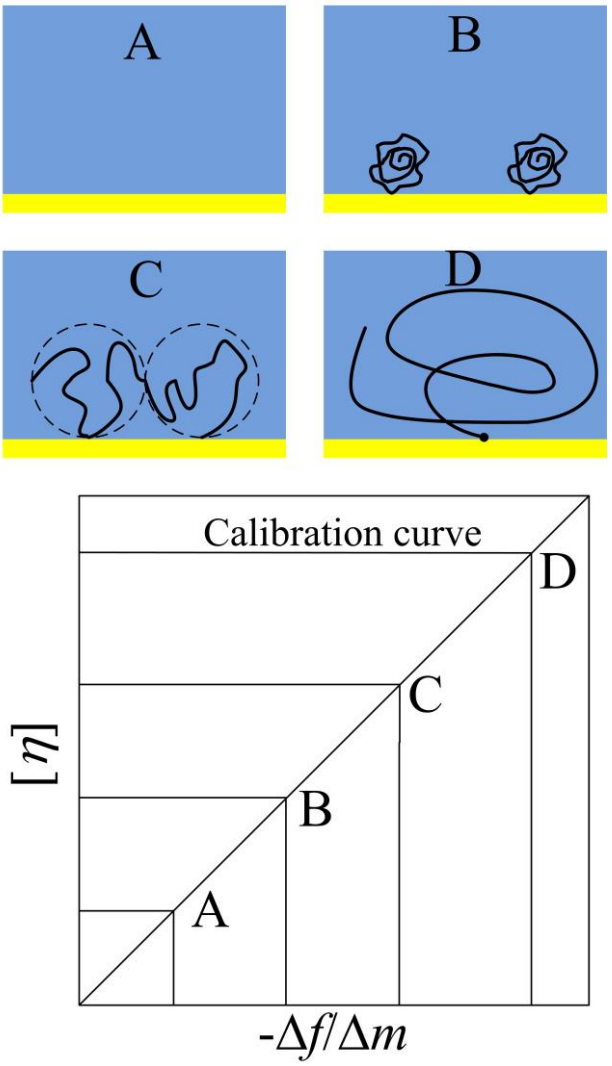

Fig. 3 The qualitative relation between the conformation of discrete chains at solid-liquid interfaces and the value of $-\Delta f/\Delta m$. A: viscous fluid, B: end-grafted compact molecules, C: physisorbed coil molecules. D: end-grafted coil molecules.

The conformation measurement of discrete adsorbates at solid-liquid interfaces based upon equation 25 can be further expanded. This is qualitatively shown in Figure 4. Curves A and B represent the coil-globule-coil transition of the discrete end-grafted chain. Such transition can be induced by changing temperature, pH, etc. Curve C means the size of the chain directly adsorbed from the aqueous solution at the same condition. Figure 4D shows the corresponding variation of Δf, or $-\Delta f/\Delta m$, since Δm keeps constant in such process. In the past, because of the ambiguous physical meaning of Δf, a comprehensive analysis of such process is hard. But now from equation 25, it is clear that the variation of Δf implies the change of intrinsic viscosity, or in other words, the size, of discrete adsorbates. The possible difference of Δf between curves A and B exposes the conformation hysteresis, while that between curves A and C reveals the influence of dimensional confinement on the ability of conformational responsiveness to external stimuli.

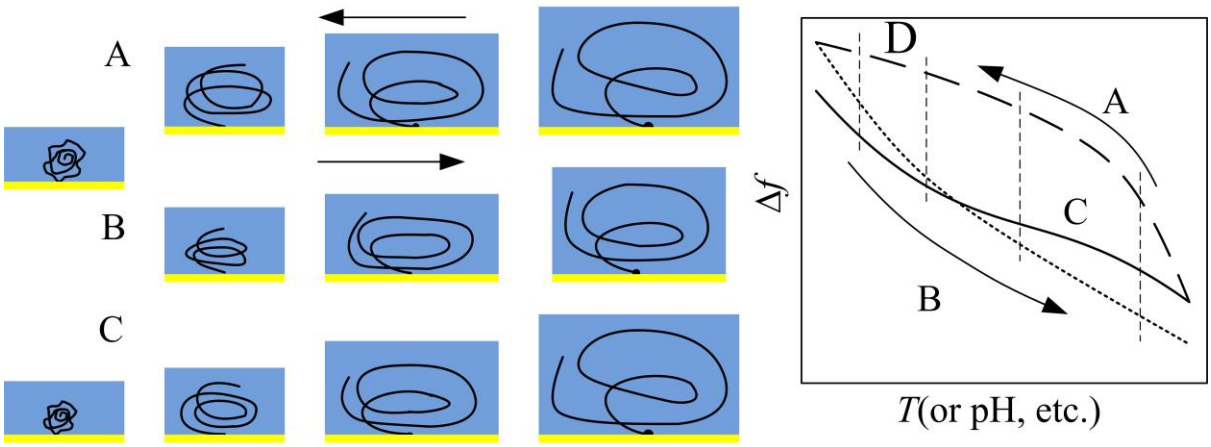

Fig. 4 Sketched plots showing the effect of the dimensional confinement, etc., on the conformational change of the flexible molecules at solid-liquid interfaces.

IV.5 QCM: Qualitative Characterization of Conformation Change from Energy Loss View

The specific relation between ΔD and Δf has been frequently used to probe the conformation of adsorbates at solid-liquid interfaces. The physics behind this method is quite simple: Δf is proportional to areal mass, $\Delta D/(-\Delta f)$ exhibits the energy loss per unit mass of adsorbates.[26,27] Large and small values of $\Delta D/(-\Delta f)$ indicate viscous and rigid adsorbed layers, and coil and globule states of adsorbates, respectively. Figure 5 qualitatively shows the relation between the slope in ΔD - $(-\Delta f)$ plot and the conformation of discrete adsorbates in the case of a small surface coverage and a minimal hydrodynamic interactions between adsorbates.[30] Typical applications include the measurement of structural change and phase behavior of the chains during adsorption,[46] the conformation of thermoresponsive polymer brush,[47] and pancake-mushroom-brush transition of adsorbed polymers.[48]

Two relationships between $\Delta D/(-\Delta f)$ and Δf have been reported. Gizeli et al. found that for end-grafted ds-DNA, $\Delta D/(-\Delta f)$ depends on the shape, length L (or base pair number), and the bending point of ds-DNA, regardless of the grafting density.[30] For straight ds-DNA, $\Delta D/(-\Delta f) \sim L^{\alpha}$. They deemed that $\Delta f \sim \Delta m$, $\Delta D \sim [\eta]\Delta m$, and $\Delta D/(-\Delta f) \sim [\eta] \sim L^{\alpha}$. They used this ratio to distinguish the different shapes and sizes of DNA, as well as study DNA conformation in hybridization processes.[30]

The other relationship is that $\Delta D/(-\Delta f)$ decreases linearly with increasing $-\Delta f$. The value of $-\Delta f$ when $\Delta D/(-\Delta f)$ approaches zero is proportional to the size of the adsorbates.[16,31] Therefore, the height distribution and average particle diameter can be obtained. This proposed method is supposed to be independent of adsorbed molecule geometry and surface packing geometry,

and can be used to study the orientation of deposited molecules.[31]

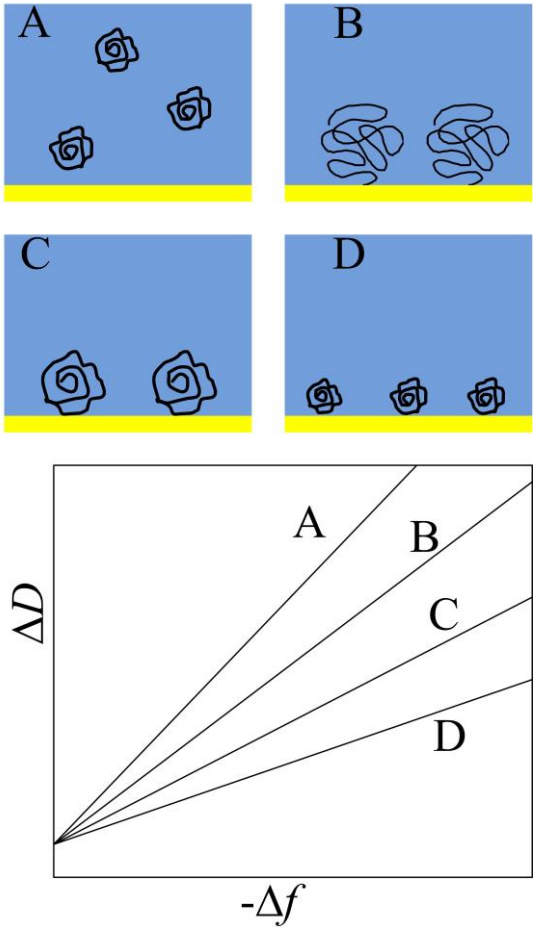

Fig. 5 The relation between the conformation of chains at solid-liquid interfaces and the corresponding ΔD - ($-\Delta f$) curve. A: viscoelastic or viscous boundary solution, B: coil chain, C: semi-coil chain, D: globule chain.

The imperfections of such method are that, on one hand, a universal experimental relation between $\Delta D/(-\Delta f)$ and $-\Delta f$ has not been found. It remains ambiguous what property of adsorbed chains results in the change of $\Delta D/(-\Delta f)$ with increasing $-\Delta f$. On the other hand, in the liquid phase, no simple proportional relation between Δf and Δm with a constant coefficient has ever been theoretically derived. The physics of ΔD remain ambiguous today. A

large amount of theoretical works are required to explore the valuable information obtained from different experimental results.

However, the shear acoustic wave amplitude decays quickly in a soft medium and slowly in a solid, as shown in Figure S5. From this, ΔD relates to the conformation, compact or extended, solid or soft, of chains at solid-liquid interfaces.

In addition, $\Delta D = 0$ indicates a solid layer. In this case, Δf is proportional to the layer thickness with a constant coefficient, as will be discussed below. Therefore, although it is not clear why the decrease of $\Delta D/(-\Delta f)$ should be linear, it is not surprising that the size of rigid molecules can be obtained from the value of $-\Delta f$ when $\Delta D/(-\Delta f)$ approaches zero.

One point that needs to be emphasized is that this method of conformation measurement is completely different from that of the value of $-\Delta f/\Delta m$. From the theoretical view, we bridge intrinsic viscosity, a concept that was presented decades ago, and the flexible value of $-\Delta f/\Delta m$. This method has definite hypotheses and a clear physical meaning. Contrary to this, the physical meaning of $\Delta D/(-\Delta f)$ is ambiguous. From the applied view, the method of $\Delta f/\Delta m$ requires a low surface coverage and a linear relation between surface viscosity and mass. The independent variable is mass. The method of $\Delta D/(-\Delta f)$ refers to both the discrete and crowded states of adsorbates. The independent variable can be either the conformation or the mass.

V VISCOELASTIC PROPERTIES OF AN ADSORBED LAYER

As pointed out above, the thickness, h_f, density, ρ_f, shear viscosity, η_f, and modulus, μ_f, of an adsorbed layer were introduced to give a reasonable interpretation of Δf and ΔD. It is natural to try to calculate these properties from Δf and ΔD.

However, it is impossible to obtain three parameters from measured Δf and ΔD. A compromise is to fit equations S6 and S7 with Δf and ΔD under different overtones (3, 5, 7, 9, 11, and 13) to obtain the most optimized η_f, μ_f and m_f (or h_f). In such fittings, the layer is assumed homogeneous. The shear viscosity and modulus are independent of shear frequency, or the relations are stated beforehand with several variables. For example, within a limited frequency range, they are approximated by power laws with exponent α_1 and α_2, $\eta = \eta_0(\omega/\omega_0)^{\alpha 1}$, and $\mu = \mu_0(\omega/\omega_0)^{\alpha 2}$, where ω_0 is an arbitrarily chosen reference frequency.[28] It is very easy for users to determine η_f, μ_f and m_f (h_f), and parameters such as α_1 and α_2. A detailed description of these algorithms can be found elsewhere.[26-28]

A limitation of this method is that, both theoretical and experimental studies have proved surface concentration at solid-liquid interfaces decreases with increasing distance to the sensor surface. This also holds true for viscosity and shear modulus. In addition, the assumption that the viscosity and shear modulus are frequency-independent or the dependency follows power laws is valid only in a small frequency range. Additionally, coupling of the material to the surface of QCM sensor leads to additional relaxation, making the relation between viscoelastic properties and shear frequency more complex.

The significance of this method lies in the lack of ways to estimate the viscoelastic properties of a thin film at solid-liquid interfaces, simply and quantitatively. Parameters calculated from the Voight model can be considered as the effective properties (h_{eff}, η_{eff}, and μ_{eff}) of the ideal layer (the viscoelastic properties are homogenous and shear frequency independent) which results in the same Δf and ΔD. The process is shown in Figure 6. Though the detailed relations between the effective and actual properties are not clear, it is reasonable

that different actual properties lead to different Δf and ΔD, and thus different effective properties.

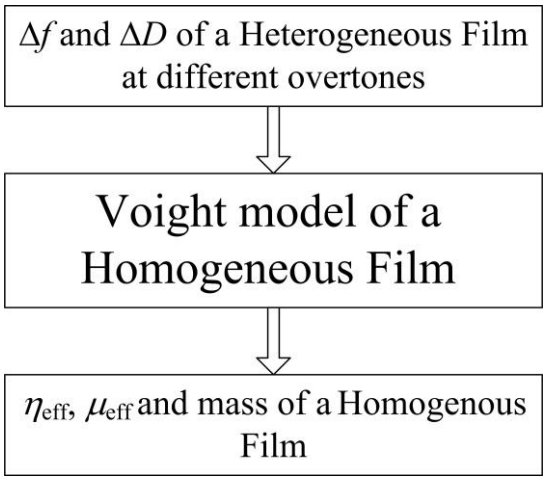

Fig. 6 Calculation of the viscoelastic properties of a thin film at solid-liquid interfaces.

VI MOLECULAR RULER AND CONTACTING METHOD

Thickness is one important parameter of the film. For physisorbed polymers and biomolecules at solid-liquid interfaces, the layer thickness provides a simple estimation of the size of an adsorption blob. The effect of adsorption force on the size of an adsorption blob can also be probed.[6] For end-grafted or surface initiated polymerized polymer brushes, this is a convenient way to study how the thickness responds to external stimuli.[47]

SPR technique provides the maximum mass and number (Δm_{max} and N_{max}) of adsorbed molecules. For flexible molecules, which do not have a definite relation between N_{max} and layer thickness, SPR signal cannot provide the thickness without calibration. If the molecules are rigid, there is at least a relation between N_{max} and the averaged surface occupied by a single molecule, *s*, where

$$s = 1/N_{max} = MN_A \frac{4\pi}{\lambda}\left(\frac{\varepsilon_m}{\varepsilon_m + \varepsilon_b}\right)^2\left(-\frac{\varepsilon_b}{\varepsilon_m}\right)^{1/2}\frac{dn}{dc}/\Delta\theta_{max} \quad (26)$$

where N_A is Avogadro's number. The contacting surface or orientation can be obtained from the value of s. For a particle of length a, width b, and height c ($a \geq b \geq c$), the relation between s and the contacting surface is shown in Table 2 and Figure 7. With increasing differences between the length, width and height of the rigid molecules, the ratio of blank space between adjacent molecules to occupied space decreases, and the precision of this method increases.

For QCM technique, if the layer is dense, which means

$$\mu_f^2 + \eta_f^2\omega^2 >> \eta_b\eta_f\omega \quad (27)$$

from Voight model,[27] we have

$$h_f \approx -m_q\Delta f / f\rho_f \quad (28)$$

Currently, QCM is an alternative tool to characterize the film thickness by virtue of its acoustic principle to measure mass and viscoelastic properties of adsorbed layer. This conclusion has been verified by experimental results. For example, the values of Δf are -13 Hz and -26 Hz for lipid monolayer and bilayer, respectively.[51] For the polymer film at solid-liquid interfaces, a reasonable assumption is often $\rho_f \approx 1$ g/cm^3. In this case for commonly used 5 MHz crystal sensor, 1 Hz shift in f indicates a 0.17 nm change in thickness. This technique of estimating the film thickness is named the "molecular ruler".[52]

For irregular rigid molecules, information such as the contacting surface and orientation can be obtained. Table 2 and Figure 7 show how to retrieve this information from Δf_{max}. This estimation is consistent with the evaluation of particle size from the value of Δf when ΔD approaches zero.[16,31]

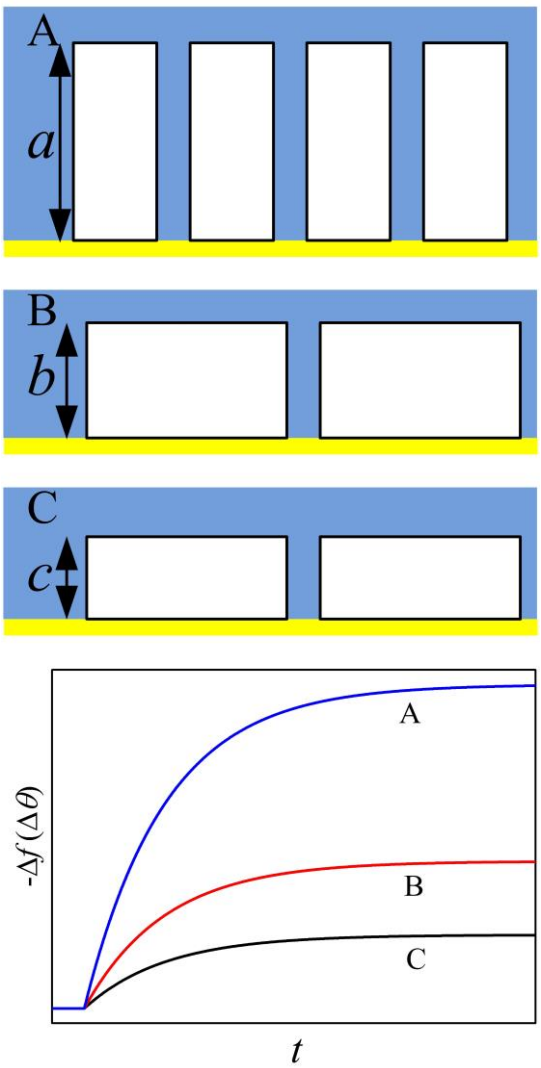

Fig. 7 Relationships between $\Delta\theta_{max}$ and Δf_{max}, and the contacting surface of rigid molecules of size *a*, *b*, and *c*, at solid-liquid interfaces.

Table 2 Relationships between the average surface area of every molecule from SPR technique, the thickness of an adsorbed film from QCM, and the contacting surface of the rigid molecules with length *a*, width *b*, and height *c* at solid-liquid interfaces.

Signals	Contacting surface
$s < ac$	bc

$b < -m_q\Delta f/f\rho_f$

$ac << s < ab$ ac

$c < -m_q\Delta f/f\rho_f < b$

$ab <$ s ab

$-m_q\Delta f/f\rho_f < c$

VII DETECTION LIMIT AND MASS AMPLIFICATION

Mass sensitivity may be the most important parameter of a mass sensor. To enhance it, common methods include improving the quality factor,[53] modifying the surface with a functional film to enhance the capture efficiency or binding constant,[43] and linking the target molecule with other molecule to amplify the mass.[54] However, for each measurement technique, there are improvements based on a technique's specific response mechanism that cannot be used by others. We discuss such methods for QCM and SPR techniques below.

From equations S3 and S4, a larger value of $[\varepsilon_m/(\varepsilon_m + \varepsilon_b)]^2(-\varepsilon_b/\varepsilon_m)^{1/2}$ indicates a higher sensitivity of SPR measurement. Figure 8 shows that it increases slightly with increasing ε_b and decreasing ε_m, since their variable ranges are just tens of percent.

From equation S5, the sensitivity (mass change for a 1 Hz shift of f) increases exponentially with a factor of 2 when f is increased, since $m_q \sim 1/f$. In this case, with f increases from 5 MHz to 5 GHz, the sensitivity increases from 17.7 ng/cm^2 to 17.7 fg/cm^2.

Such method has been adopted long ago.[55] The highest resonant frequency reported is 180 MHz.[56] Uttenthaler et al. created crystals operating in the 19 - 119 MHz range.[57] They showed empirically that f and mass change relationship has in fact a larger exponent of 2.88.

Furthermore, there is a 200-fold improvement in detection sensitivity for M13 phase binding to the 56 MHz crystals compared to the same system on 19 MHz crystals. These results indicate a more dramatic thickness dependence of mass and detection sensitivity of QCM technique than theoretically predicted.

However, with increasing *f*, (1) the sensor becomes increasingly fragile, the thickness should be thus larger than one specific value to ensure an excellent oscillation in liquid phase, (2) the penetration depth of shear acoustic wave decreases, indicating a smaller measured thickness regime on top of sensor surface, (3) the difficulty of the precise measurement of the oscillation amplitude increases, the investigators may have to build their own oscillator circuits, (4) the liquid properties begin to affect the results. These may be why the maximum *f* of commonly used quartz crystal is 27 MHz.

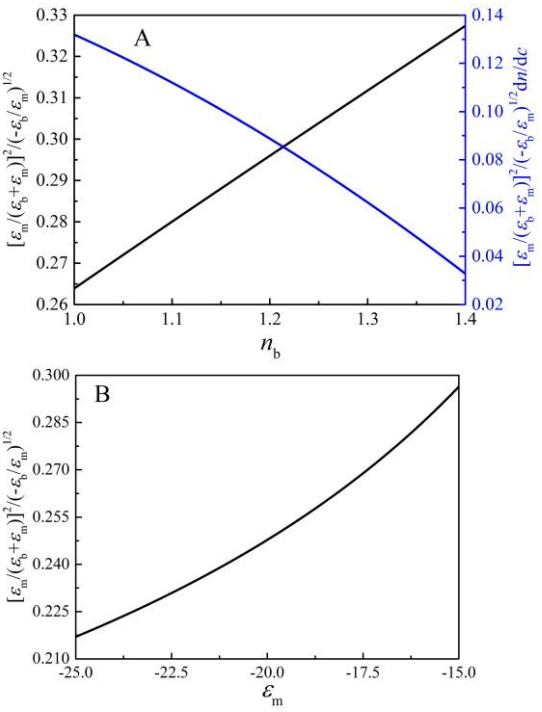

Fig. 8 (A) dependences of $[\varepsilon_m/(\varepsilon_m + \varepsilon_b)]^2(-\varepsilon_b/\varepsilon_m)^{1/2}$ and $[\varepsilon_m/(\varepsilon_m + \varepsilon_b)]^2(-\varepsilon_b/\varepsilon_m)^{1/2}dn/dc$ on the refractive index of the background, ε_m = - 18.05, and (B) dependence of $[\varepsilon_m/(\varepsilon_m + \varepsilon_b)]^2(-\varepsilon_b/\varepsilon_m)^{1/2}$ on ε_m, n_b = 1.333.

At the same time, $\Delta\theta$ and Δf are proportional to dn/dc and [η] of adsorbed molecules (equations S4 and 25), respectively. For SPR technique, the ideal solvent is one in that dn/dc is large. Figure 11A shows that $[\varepsilon_m/(\varepsilon_m + \varepsilon_b)]^2(-\varepsilon_b/\varepsilon_m)^{1/2}dn$/d$c$ increases by approximately a factor of four, when n_b decreases from 1.4 to 1. Here dn/dc = 1.5 - n_b, where 1.5 is assumed to be the refractive index of the species investigated. To obtain the maximum sensitivity for QCM technique, the ideal solvent is one in that the molecule is extensively stretched, and the ideal substrate is one where substrate-adsorbate interactions are the weakest (i.e., the molecule is end-grafted on the substrate). Therefore, the sensitivity of SPR technique in the vapor phase is larger than in the liquid phase. On the other hand, the sensitivity of QCM technique decreases significantly, as $\rho[\eta] \sim 1$ in the gas phase, and $\rho[\eta] >> 1$ in liquid phase.

The discussion above has also had a significant impact in mass amplification. Metallic nanoparticles are generally used in this process.[55] They are perfect for SPR technique, because of their high mass and high refractive index. They are not ideal for QCM technique as the intrinsic viscosity is very small. The molecules with high mass and intrinsic viscosity, such as DNA molecules of a large number of base pair (for example, T2, M = 115 M, [η] = 3.16×10^7 mL/mg[58]), are perfect for QCM techniques. For a comprehensive understanding of the effect of properties of linked molecules on the mass amplification efficiency of SPR and QCM techniques, large amount of experimental results are required.

Table 3 Summary of the Differences between SPR and QCM.

	SPR	QCM
	The detection limit of the refractive	Measures viscoelastic properties, roughly

Boundary Solution		index and polymer concentration can be about 1.7×10^{-7} and 0.8 μg/ml, respectively.	depicts the profiles of viscosity, shear modulus, and the polymer conformation as a function of the distance to the solid substrate.
Surface Modification		The thickness is less than tens of nanometers. The roughness and rigidity are not problematic.	Smooth and rigid film, with a thickness less than tens of micrometers.
Conformation of Adsorbates and Adsorbed Layer at Solid-Liquid Interfaces		From the view of the changing behavior of $\Delta\theta$ at fixed Δm, qualitative.	From the view of the changing behavior of Δf, qualitative.
			From the view of energy loss per unit mass, qualitative.
			From the relation between Δf and Δm and other similar relations, qualitative.
			From intrinsic viscosity view, quantitative. The unique application of QCM.
Viscoelastic Properties of Film		No.	Qualitative.
Molecular Ruler	Thickness of Dense Film	No.	Yes.
	Contacting Surface of Irregular Rigid Molecules	From surface area occupied by single molecules at saturated adsorption, qualitative.	From thickness at saturated adsorption, qualitative.
Mass Sensitivity Enhancement	Solvent	Improved slightly by decreasing the refractive index of the solvent.	Improve ten times by selecting a solvent that sufficiently stretches the molecule
	From Gas to Liquid Phase	Decreased by several times.	Mass sensitivity can be improved by one to two orders of magnitude.
	Parameters of the Equipment	Improved slightly by decreasing dielectric constant of metallic film.	Improved by several orders of magnitude by improving *f*.
	Mass Amplification	Prefers molecules of large refractive index and mass.	Prefers molecules of large intrinsic viscosity and molecular weight.

VIII CONCLUSIONS

The increasing popularity of the combination of surface plasmon resonance and quartz crystal microbalance techniques reveals the power of this combination for probing the phenomena that take place at solid-liquid interfaces. Large amount of information, such as areal mass, conformation (solvation, hydrodynamic effects, intrinsic viscosity and lateral distribution), film thickness, contacting surface and orientation, viscoelastic properties, of adsorbates and adsorbed layer at solid-liquid interfaces can be extracted. In this paper, based on theoretical calculations and analysis, we have outlined the different types of information that can be obtained, why it can be obtained, and how to obtain it, with SPR and QCM techniques in various experimentally relevant scenarios. The major results are summarized in Table 3.

Additionally, for evaluating the conformation through QCM, we also: (1) showed the origins of the current phenomenological interpretations and why they are imperfect, (2) provided one explanation as to why the resonant frequency shift is sensitive to conformational change, based on the relation between surface viscosity and surface concentration, (3) offered one method to quantitatively probe the conformation of discrete polymers and biomolecules at solid-liquid interfaces.

This paper has also formulated the guidelines for designing proper experimental procedures in different situations, such as calibrating the effect of a modified surface, and quantifying the mass amplification efficiency before the experiments. Numerous experiments are required to demonstrate how to obtain the information of the phenomena occurring at solid-liquid interfaces as accurate as possible, from the combination of SPR and QCM

techniques.

ACKNOWLEDGMENTS

This work was supported by the National Basic Research Program of China (No. 2012CB821500) and the National Natural Science Foundation of China (Nos. 91027040, 31061160496, 11104192, and 21264016).

Notes and References

† Electronic Supplementary Information available: A detailed description of the theory of SPR and QCM techniques, the dependences of their signals on the properties of layer above their sensor surfaces, and the different propagation characters of evanescent and shear acoustic waves in different mediums.

(1) For representative examples, see: (a) R. J. Gibbons, *J. Dent. Res*., 1989, **68**, 750-760. (b) J. S. Kim, *J. Neurol. Sci*., 1996, **137**, 69-78. (c) D. M. Touart, P. J. Sau, *Am. Acad. Dermatol*., 1998, **39**, Part I: 149-171. Part II: 527-546. (d) J. Muller, G. Wallukat, M. Dandel, H. Bieda, K. Brandes, S. Spiegelsberger, E. Nissen, R. Kunze, R. Hetzer, *Circulation*, 2000, **101**, 385-391.

(2) (a) Z. Y. Tang, Y. Wang, P. Podsiadlo, N. A. Kotov, *Adv. Mater*., 2006, **18**, 3203-3224. (b) R. A. Scott, A. Panitch, *Biomacromolecules*, 2014, **15**, 2825-2832.

(3) (a) B. Thierry, F. M. Winnik, Y. Merhi, M. Tabrizian, *J. Am. Chem. Soc*., 2003, **125**, 7494-7495. (b) T. Groth, A. Lendlein, *Angew. Chem. Int. Ed*., 2004, **43**, 926-928.

(4) (a) B. Kasemo, J. Gold, *Adv. Dent. Res*., 1999, **13**, 8-20. (b) C. J. Wilson, R. E. Clegg, D. I. Leavesley, M. J. Pearcy, *Tissue Eng*., 2005, **11**, 1-18.

(5) (a) M. A. Cohen Stuart, W. T. S. Huck, J. Genzer, M. Muller, C. Ober, M. Stamm, G. B. Sukhorukov, I. Szleifer, V. V. Tsukruk, M. Urban, F. Winnik, S. Zauscher, I. Luzinov, S. Minko, *Nat. Mater*., 2010, **9**, 101-113. (b) T. Chen, R. Ferris, J. M. Zhang, R. Ducker, S. Zauscher, *Prog. Polym. Sci*., 2010, **35**, 94-112.

(6) M. Rubinstein, R. H. Colby, *Polymer Physics*, Oxford University Press: Oxford, 1st ed.; 2003.

(7) C. A. Keller, K. Glasmastar, V. P. Zhdanov, B. Kasemo, *Phys. Rev. Lett*., 2000, **84**, 5443-5446.

(8) F. Hook, B. Kasemo, T. Nylander, C. Fant, K. Sott, H. Elwing, *Anal. Chem*., 2001, **73**, 5796-5804.

(9) F. Hook, J. Voros, M. Rodahl, R. Kurrat, P. Boni, J. J. Ramsden, M. Textor, N. D. Spencer, P. Tengvall, J. Gold, B. Kasemo, *Colloids Surf. B*, 2002, **24**, 155-170.

(10) L. E. Bailey, D. Kambhampati, K. K. Kanazawa, W. Knoll, C. W. Frank, *Langmuir*, 2002, **18**, 479-489.

(11) A. Granli, J. Rydstrm, B. Kasemo, F. Hook, *Langmuir*, 2003, **19**, 842-850.

(12) E. Reimhult, C. Larsson, B. Kasemo, F. Hook, *Anal. Chem*., 2004, **76**, 7211-7220.

(13) X. D. Su, Y. J. Wu, R. Robelek, W. Knoll, *Langmuir*, 2005, **21**, 348-353.

(14) E. Reimhult, M. Zach, F. Hook, B. Kasemo, *Langmuir*, 2006, **22**, 3313-3319.

(15) P. Bingen, G. L.Wang, N. F. Steinmetz, M. Rodahl, R. P. Richter, *Anal. Chem*., 2008, **80**, 8880-8890.

(16) D. Johannsmann, I. Reviakine, R. P. Richter, *Anal. Chem*., 2009, **81**, 8167-8176.

(17) M. Edvardsson, S. Svedhem, G. L.Wang, R. P. Richter, M. Rodahl, B. Kasemo, *Anal. Chem*., 2009, **81**, 349-361.

(18) I. Carton, A. R. Brisson, R. P. Richter, *Anal. Chem*., 2010, **82**, 9275-9281.

(19) C, M. Zhou, J. J. Fang, D. Y. Chen, will submitted to *Physical Review E*.

(20) B. Liedberg, C. Nylander, I. Lunstrom, *Sens. Actuators*, 1983, **4**, 299-304.

(21) B. Liedberg, I. Lundstrom, E. Stenberg, *Sens. Actuators B*, 1993, **11**, 63-72.

(22) L. S. Jung, C. T. Campbell, T. M. Chinowsky, M. N. Mar, S. S. Yee, *Langmuir*,1998, **14**, 5636-5648.

(23) For representative examples, see: (a) H. Sota, Y. Hasegawa, M. Iwakura, *Anal. Chem*., 1998, **70**, 2019-2024. (b) S. Boussaad, J. Pean, N. J. Tao, *Anal. Chem*., 2000, **72**, 222-226. (c) J. E. Gestwichi, H. V.

Hsieh, J. B. Pitner, *Anal. Chem*., 2001, **73**, 5732-5737. (d) S. Balamurugan, S. Mendez, S. S. Balamurugan, M. J. O'Brien II, G. P. Lopez, *Langmuir*, 2003, **19**, 2545-2549.

(24) G. Sauerbrey, *Z. Phys*., 1959, **155**, 206-222.

(25) (a) M. Muratsugu, F. Ohta, Y. Miya, T. Hosokawa, S. Kurosawa, N. Kamo, H. Ikeda, *Anal. Chem*., 1993, **65**, 2933-2937. (b) T. Ozeki, M. Morita, H. Yoshimine, H. Furusawa, Y. Okahata, *Anal. Chem*., 2007, **79**, 79-88. (c) H. Furusawa, T. Ozeki, M. Morita, Y. Okahata, *Anal. Chem*., 2009, **81**, 2268-2273.

(26) M. Rodahl, B. Kasemo, *Sens. Actuators A*, 1996, **54**, 448-456.

(27) M. V. Voinova, M. Rodahl, M. Jonson, B. Kasemo, *Phys. Scr*., 1999, **59**, 391-399.

(28) D. Johansmann, *Macromol. Chem. Phys*., 1999, **200**, 501-516.

(29) J. Kankare, *Langmuir*, 2002, **18**, 7092-7094.

(30) (a) A. Tsortos, G. Papadakis, E. Gizeli, *Biosens. Bioelectron*., 2008, **24**, 836-841. (b) A. Tsortos, G. Papadakis, K. Mitsakakis, K. A. Melzak, E. Gizeli, *Biophys. J*, 2008, **94**, 2706-2715.

(31) A. L. J. Olsson, I. R. Quevedo, D. Q. He, M. Basnet, N. Tufenkji, *ACS Nano*, 2013, **7**, 7833-7843.

(32) D. Johannsmann, I. Reviakine, E. Rojas, M. Gallego, *Anal. Chem*., 2008, **80**, 8891-8899.

(33) (a) B. Wu, K. Wu, P. Wang, D. M. Zhu, *J. Phys. Chem. C*, 2007, **111**, 1131-1135. (b) K. Wu, B. Wu, P. Wang, Y. Hou, G. Z. Zhang, D. M. Zhu, *J. Phys. Chem. B*, 2007, **111**, 8723-8727. (c) D. M. Zhu, K. Wu, B. Wu, P. Wang. J. J. Fang, Y. Hou, G. Z. Zhang, *J. Phys. Chem. C*, 2007, **111**, 18679-18686.

(34) T. Zhu, Z. Y. Jiang, Y. Q. Ma, *Appl. Phys. Lett*. 2013, **102**, 153109.

(35) B. Yuan, T. Zhu, Z. X. Zhang, Z. Y. Jiang, Y. Q. Ma, *J. Mater. Chem*., 2011, **21**, 3471-3476.

(36) (a) T. Zhu, F. Xu, B. Yuan, C. L. Ren, Z. Y. Jiang, Y. Q. Ma, *Colloid Surf. B*, 2012, **89**, 228-233. (b) T. Zhu, Z. Y. Jiang, EI. M. R. Nurlybaeva, J. Sheng, Y. Q. Ma, *Langmuir*, 2013, **29**, 6377-6385.

(37) T. Zhu, Z. Y. Jiang, Y. Q. Ma, *Colloid Surf. B*. 2012, **97**, 155-161.

(38) (a) P. Wang, J. J. Fang, Y. Hou, X. B. Du. D. M. Zhu, *J. Phys. Chem. C*, 2009, **113**, 729-735. (b) P. Wang, J. J. Fang, S. Qin, Y. H. Kang, D. M. Zhu, *J. Phys. Chem. C*, 2009, **113**, 13793-13800. (c) J. J. Fang, T. Zhu, Z. Y. Jiang, Y. Q. Ma, *Sci. Rep*, Submitted.

(39) (a) D. M. Zhu, J. J. Fang, B. Wu, X. B. Du, *Phys. Rev. E*, 2008, **77**, 031605 1-7. (b) J. J. Fang, D. M. Zhu, *Phys. Rev. E*, 2008, **78**, 031604 1-8. (c) J. J. Fang, P. Wang, X. B. Du. D. M. Zhu, *J. Phys. Chem. C*, 2009, **113**, 16121-16127.

(40) J. J. Fang, C. L. Ren, T. Zhu, Z. Y. Jiang, Y. Q. Ma, *Analyst*, Submitted.

(41) For typical examples, see (a) A. Saluja, D. S. Salonia, *AAPS PharmsciTech*., 2004, **5**, 1-14. (b) G. McHale, C. Hardacre, R. Ge, N. Doy, R. W. K. Allen, J. M. MacInnes, M. R. Bown, M. I. Newton, *Anal. Chem*., 2008, **80**, 5806-5811.

(42) K. K. Kanazawa, J. G. Gordon II, *Anal. Chem*., 1985, **57**, 1770-1771.

(43) (a) W. Kim, J. K. Ng, M. E. Kunitake, B. R. Conklin, P. D. Yang, *J. Am. Chem. Soc*., 2007, **129**, 7228-7229. (b) S. T. Wang, K. Liu, J. Liu, Z. T. F. Yu, X. W. Xu, L. B. Zhao, T. Lee, E. K. Lee, J. Reiss, Y. K. Lee, L. W. L. Chung, J. T. Huang, M. Rettig, D. Seligson, K. N. Duraiswamy, C. K. F. Shen, H. R. Tseng, *Adv. Mater*., 2011, **50**, 3084-3088.

(44) (a) C. Hennesthal, C. Steinem, *J. Am. Chem. Soc*., 2000, **122**, 8085-8086. (b) P. Jonsson, M. P. Jonsson, F. Hook, *Nano Lett*., 2010, **10**, 1900-1906.

(45) H. L. Liu, Y. Y. Li, K. Sun, J. B. Fan, P. C. Zhang, J. X. Meng, S. T. Wang, L. Jiang, *J. Am. Chem. Soc*., 2013, **135**, 7603-7609.

(46) F. Hook, M. Rodahl, B. Kasemo, P. Brzezinski, *Proc. Natl. Acad. Sci. USA*, 1998, **95**, 12271-12276.

(47) (a) G. Z. Zhang, *Macromolecules*, 2004, **37**, 6553-6557. (b) G. M. Liu, G. Z. Zhang, *J. Phys. Chem. B*, 2005, **109**, 743-747.

(48) (a) G. M. Liu, H. Cheng, L. F. Yan, G. Z. Zhang, *J. Phys. Chem. B*, 2005, **109**, 22603-22607. (b) G. M. Liu, L. F. Yan, X. Chen, G. Z. Zhang, *Polymer*, 2006, **47**, 3157-3163.

(49) For representative examples, see (a) J. T. Yang, J. F. Foster, *J. Am. Chem. Soc*., 1954, **76**, 1588-1595. (b) K. Nishida, K. Kaji, T. Kanaya, N. Fanjat, *Polymer*, 2002, **43**, 1295-1300.

(50) (a) C. Tanford, *Physical Chemistry of Macromolecules*, Wiley: New York, 1961. (b) C. R. Cantor, P. R. Schimmel, *Biophysical Chemistry*, Part II. Freeman: San Francisco, 1980.

(51) C. A. Keller, B. Kasemo, *Biophys. J*, 1998, **75**, 1397-1402.

(52) (a) H. W. Ma, J. A. He, Z. Q. Zhu, B. E. Lv, D. Li, C. H. Fan, J. Fang, *Chem. Commun*., 2010, **46**, 949-951. (b) M. Huang, J. A.He, J. H. Gan, H. W. Ma, *Colloids Surf. B*, 2011, **85**, 92-96.

(53) For typical examples, see: (a) S. S. Verbridge, H. G. Craighead, J. M. Parpia, *Appl. Phys. Lett*., 2008, **92**, 013112 1-3. (b) A. K. Huttel, G. A. Steele, B. Witkamp, M. Poot, L. P. Kouwenhoven, H. S. J. van der Zant, *Nano Lett*., 2009, **9**, 2547-2552.

(54) There are numerous examples, for a brief summary, see: (a) M. A. Cooper, V. T. Singleton, *J. Mol. Recognit*., 2007, **20**, 154-184. (b) B. Becker, M. A. Cooper, *J. Mol. Recognit*., 2011, **24**, 865-787.

(55) Z. X. Lin, C. M. Yip, I. S. Joseph, M. D. Ward, *Anal. Chem*., 1993, **65**, 1546-1551.

(56) H. Ogi, T. Yanagida, M. Hirao, M. Nishiyama, *Biosens. Bioelectron*., 2011, **26**, 4819-4822.

(57) E. Uttenthaler, M. Schraml, J. Mandel, S. Drost, *Biosens. Bioelectron*., 2001, **16**, 735-743.

(58) I. N. Serdyuk, N. R. Zaccai, J. Zaccai, *Methods in Molecular Biophysics: Structure, Dynamics, Function*, Cambridge University Press, Cambridge, 2007, pp 476.